Available online at www.sciencedirect.com
SCIENCE DIRECT®
ELSEVIER
International Journal of Solids and Structures 42 (2005) 6586–6609
INTERNATIONAL JOURNAL OF SOLIDS and STRUCTURES
www.elsevier.com/locate/ijsolstr

Development of the large increment method for elastic perfectly plastic analysis of plane frame structures under monotonic loading

W.S. Barham, A.J. Aref *, G.F. Dargush

Department of Civil, Structural, and Environmental Engineering, State University of New York at Buffalo, Buffalo, NY 14260, USA

Received 31 July 2004; received in revised form 6 June 2005
Available online 20 July 2005

Abstract

The displacement-based finite element method dominates current practice for material nonlinear analysis of structures. However, there are several characteristics that may limit the effectiveness of this approach. In particular, for elastoplastic analysis, the displacement method relies upon a step-by-step incremental approach stemming from flow theory and also requires significant mesh refinement to resolve behavior in plastic zones. This leads to computational inefficiencies that, in turn, encourage the reconsideration of force-based approaches for elastoplastic problems.

One of these force algorithms that has been recently developed is the large increment method. The main advantage of the flexibility-based large increment method (LIM) over the displacement method is that it separates the global equilibrium and compatibility equations from the local constitutive relations. Consequently, LIM can reach the solution in one large increment or in a few large steps, thus, avoiding the development of cumulative errors. This paper discusses the extension of the large increment methodology for the nonlinear analysis of plane frame structures controlled by an elastic, perfectly plastic material model. The discussion focuses on the power of LIM to handle these nonlinear problems, especially when plastic hinges form in the frame and ultimately as the structure approaches the collapse stage. Illustrative planar frame examples are presented and the results are compared with those obtained from a standard displacement method.

Keywords: Planar frames; Monotonic loading; Nonlinear analysis; Displacement method; Force method; Large increment method (LIM); Elastic-perfectly plastic material model; Generalized inverse

* Corresponding author. Tel.: +1 716 645 2114x2423; fax: +1 716 645 3733.
E-mail address: aaref@eng.buffalo.edu (A.J. Aref).

0020-7683/$ - see front matter © 2005 Elsevier Ltd. All rights reserved.
doi:10.1016/j.ijsolstr.2005.06.020

Nomenclature

B	strain–displacement matrix
C^{e}	element equilibrium matrix
C	equilibrium matrix of structure
C_R^{-1}	generalized inverse of matrix C
D	generalized nodal displacement
F	generalized inner force vector of whole system
I	identity matrix
M_{p}	maximum fully plastic moment of the section
M_{y}	fully elastic moment of the section
N_{p}	maximum fully plastic normal force of the section
N_{y}	fully elastic normal force of the section
P	generalized node load vector
Q	nodal displacement shape function
S	vector of search direction
X	arbitrary vector of dimension n
Z	stress shape function
b	beam cross-sectional width
$\hat{b}$	body force vector
d	nodal displacement variable
$e(\delta_n)$	error criteria for compatibility condition at iteration n
f	generalized force variable
f_{e_i}	element forces of element i
h	beam cross-sectional height
h_n	multiplier along the search direction S_n
l	degree of indeterminacy
m	dimension of the generalized nodal displacement vector
n	dimension of the generalized inner force vector of whole system
q	total number of elements ends
r	number of element rigidity
$\hat{t}$	external traction vector
Θ	eigenvectors
$K'(\delta)$	current stiffness matrix for the whole system
$\Phi'(\delta)$	current flexibility stiffness matrix for the whole system
χ_{p}	cross-sectional fraction at the yield stress
α	$n \times n$ matrix related to C
β	$n \times n$ matrix related to C
δ	generalized deformation vector for whole system
δ_{e_i}	deformation variables of element i
δ^{p}	plastic deformation
ε	strain tensor
ε^{p}	plastic strain tensor
ρ	number of elements
η	variable index
θ_{p}	plastic hinge rotation

$\kappa'(\delta)$	element stiffness matrix
$\kappa'_{\text{reduced}}(\delta)$	element reduced stiffness matrix
λ	diagonal eigenvalue matrix
λ_{reduced}	reduced diagonal eigenvalue matrix
μ	applied force size factor
ξ_{p}	plasticity index
ξ_{e}	elasticity index
ζ	dimensionless plastic hinge locator
σ	stress tensor
σ_{y}	yield stress
$\phi'(\delta)$	element flexibility matrix
$\phi'_{\text{reduced}}(\delta)$	element reduced flexibility matrix
φ	generalized deformation function

1. Introduction

With the advancement in computer technology, many researchers direct their efforts toward nonlinear analysis of structures. In this field, two major approaches have been adopted. The displacement based finite element approach (Turner et al., 1956; Clough, 1960; Oden, 1972; Cook et al., 1989; Bathe, 1996) and the force based finite element approach (Patnaik, 1973; Kaljevic et al., 1996; Spacone et al., 1996). The primary unknowns in the latter method are the internal element forces instead of the nodal displacements as in the former method.

The displacement approach uses a step-by-step solution procedure that depends on the decomposition of the total load into small increments. The history for all solution variables is known up to time t and the problem is to solve for the state variables at $t + \Delta t$. The Newton–Raphson method is commonly used for solving the nonlinear system of equations at $t + \Delta t$ (e.g., Bathe, 1996). Therefore, numerical errors are expected at the end of each step, which will accumulate and consequently propagate to the subsequent steps. To improve the solution quality, one needs to reduce the load step size. Additionally, significant mesh refinement is needed in the plastic zone due to the complicated variation of the deformation field within that region.

Consequently, a number of researchers have shifted their interest toward the force-based finite element (FE) approach for analyzing structural problems with nonlinear materials. The large increment method (LIM) is a forced-based FE algorithm proposed recently in Zhang and Liu (1997), Aref and Guo (2001) and Barham et al. (2003). One main advantage of this method is that it can handle the complexity of the nonlinear problem without severe restrictions on step size. This is because the nonlinearity of the problem is treated in the local stage (i.e. at the element level), while the linear equilibrium and compatibility equations are treated in the global stage. By separating these two stages there is no need to linearize the constitutive model and the load often can be handled in one large step in the case of monotonic loading. The solution of the problem is the intersection between the manifold representing the global linear stage and the manifold representing the local nonlinear stage as shown in Fig. 1.

An iterative solution procedure is adopted to reach the intersection point using information from both manifolds during the iteration. Furthermore, the generalized internal force fields often permit a more compact discretization, especially, in highly nonlinear zones. Consequently, LIM has the potential to overcome the disadvantages of the displacement method mentioned above.

A related approach was presented in Boisse et al. (1989, 1990) and Ladeveze (1999). In their work, they introduce a single large increment scheme for solving nonlinear material problems in which it is necessary to iterate for the entire loading path to account for the history of the state variables. A time decomposition is

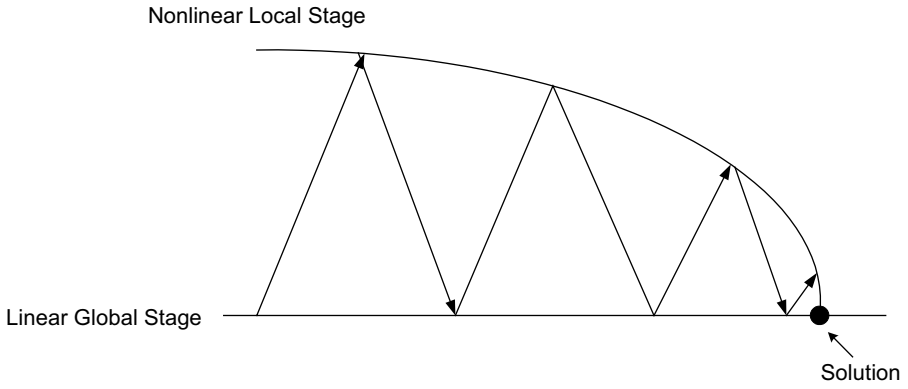

Fig. 1. Solution demonstration.

adopted to make the transformation between the local nonlinear stage and the linear global stage. On the other hand, the present LIM uses a simple procedure based upon the theory of generalized inverse of a matrix.

In this paper, the large increment algorithm is extended to analyze plane frame structures controlled by an elastic-perfectly plastic material model. In the following sections, the overall LIM approach is summarized, the generalized inverse is defined, the new elastoplastic frame element is formulated, and the solution procedure is detailed. Afterwards, illustrative examples are presented for this class of problems, and numerical results are compared with those obtained from the displacement method.

In the next section of this paper, the generalized governing equations are presented in detail in order to enable a better understanding for the large increment method in relation to this generalized matrix inverse.

2. LIM generalized governing equations

This section outlines the basic governing equations needed in the LIM formulation for a continuum. The domain occupied by the structure is denoted as Ω, and its boundary is represented as $\partial\Omega$. The boundary is divided into two parts: the displacement boundary $\partial\Omega_u$ and the traction boundary $\partial\Omega_\sigma$, where $\partial\Omega_u \cup \partial\Omega_\sigma = \partial\Omega$ and $\partial\Omega_u \cap \partial\Omega_\sigma = 0$. On the displacement boundary $\partial\Omega_u$, the displacement is constrained to be $\hat{u}$, and on the traction boundary $\partial\Omega_\sigma$, the external traction is $\hat{t}$. The equilibrium equations can be written:

$$\sigma_{ij,j} + \widehat{b_i} = 0, \quad \text{in } \Omega \tag{1}$$

in terms of the stress tensor σ and the body forces $\hat{b}$. Meanwhile, the constitutive relationships are

$$\varepsilon = \phi(\sigma, \varepsilon^{\mathrm{p}}), \tag{2}$$

where the strain tensor ε is defined by the following equation:

$$\varepsilon_{ij} = \frac{1}{2}(u_{i,j} + u_{j,i}) \tag{3}$$

and ε^{p} represents the plastic strain tensor. Meanwhile, the boundary conditions are defined now as,

$$\sigma_{ij} n_j = \widehat{t_i}, \quad \text{on } \partial\Omega_\sigma \tag{4}$$

$$u_i = \widehat{u_i}, \quad \text{on } \partial\Omega_u. \tag{5}$$

To solve the above equations, the whole system is divided into ρ discrete elements, and the generalized force variables f and node displacement variables d of each element are taken as the basic variables. The generalized force variables are related to the tractions through an integration process. The stress and displacement of each point in any element can be represented by the element generalized force variables and nodal displacement variables by using interpolation functions as follows:

$$\begin{cases} \sigma = Zf, \\ u = Qd, \end{cases} \tag{6}$$

where Z is the shape function of force variables, and Q is the shape function of nodal displacement variables. Furthermore, the strain in the element can be represented by the nodal displacement variables,

$$\begin{cases} \varepsilon_{ij} = B_{ijl} d_l, \\ B_{ijl} = (Q_{il,j} + Q_{jl,i})/2. \end{cases} \tag{7}$$

To satisfy the displacement boundary condition and the continuity of element displacement, it is required that

$$\dim f \geqslant \dim d - r, \tag{8}$$

where "dim" denotes dimension, and r is the number of element rigidity displacements.

Using the principle of virtual work, one finds

$$\int_\Omega \sigma_{ij}\, \delta\varepsilon_{ij}\, \mathrm{d}\Omega = \int_\Omega \widehat{b}_i\, \delta u_i\, \mathrm{d}\Omega + \int_{\partial\Omega_\sigma} \widehat{t}_i\, \delta u_i\, \mathrm{d}S. \tag{9}$$

Thereby, the equilibrium equations of the system are obtained as,

$$CF = P, \tag{10}$$

where C, F, P are assembled from the following components of each element:

$$\begin{cases} F = [f_{\mathrm{e}_1}, f_{\mathrm{e}_2}, \ldots, f_{\mathrm{e}_\rho}]^{\mathrm{T}}, \\ C^{\mathrm{e}} = \int_{\Omega^{\mathrm{e}}} B^{\mathrm{T}} Z\, \mathrm{d}\Omega, \\ P^{\mathrm{e}} = \int_{\partial\Omega^{\mathrm{e}}_\sigma} Q^{\mathrm{T}} \hat{t}\, \mathrm{d}S + \int_{\Omega^{\mathrm{e}}} Q^{\mathrm{T}} \hat{b}\, \mathrm{d}\Omega. \end{cases} \tag{11}$$

Here the virtual fields assume the same form as the real fields defined in (6) and (7).

Similarly, using the principle of complementary virtual work,

$$\int_\Omega (\varepsilon_{ij} - B_{ijl} d_l)\, \delta\sigma_{ij}\, \mathrm{d}\Omega = 0, \tag{12}$$

we obtain the compatibility equations of the system,

$$C^{\mathrm{T}} D = \delta, \tag{13}$$

where D is the nodal displacement vector of the system and δ denotes the element generalized deformation:

$$\begin{cases} \delta = [\delta_{\mathrm{e}_1}, \delta_{\mathrm{e}_2}, \ldots, \delta_{\mathrm{e}_\rho}]^{\mathrm{T}}, \\ \delta_{\mathrm{e}_i} = \int_{\Omega^{\mathrm{e}}_i} Z^{\mathrm{T}} \varepsilon\, \mathrm{d}\Omega. \end{cases} \tag{14}$$

Then, the constitutive relations could be written as

$$\delta = \varphi(F, \delta^{\mathrm{p}}) \tag{15}$$

and for each element,

$$\varphi_{e_i}(f_{e_i}, \delta^p) = \int_{\Omega_i^e} Z^T \varepsilon_{e_i} \, d\Omega. \tag{16}$$

Thus, the final generalized governing equations of the system are

$$\begin{cases} CF = P, \\ C^T D = \delta, \\ \delta = \varphi(F, \delta^p). \end{cases} \tag{17}$$

3. Theory of the generalized inverse of a matrix

The theory of the generalized inverse of a matrix, which was introduced in the 1950s, is a powerful mathematical tool to analyze a non-square matrix (Ben-Israel and Greville, 1974). Here the generalized inverse will be utilized to solve the linear equilibrium and compatibility equations defined by (10) and (13), where C is an $m \times n$ matrix, P is an m-dimensional vector, and F is an n-dimensional vector. Assume C and P are known and F is unknown. For statically determinate structures, $m = n$, and C is invertible (i.e. $\text{rank}(C) = m$). Thus, it is well known that F could be achieved easily as,

$$F = C^{-1}P. \tag{18}$$

For indeterminate structures, $m < n$, thus, F could not be presented as in (18) because C^{-1} will no longer exist and there will be an infinite set of vectors F satisfying (10). However, using the theory of the generalized inverse of a matrix, we can still present all the vectors satisfying (10). Assume $\text{rank}(C) = m$. Then as an $m \times m$ matrix CC^T, we will have $\text{rank}(CC^T) = m$, which means matrix $(CC^T)^{-1}$ exists. Let

$$C_R^{-1} = C^T(CC^T)^{-1} \tag{19}$$

then

$$CC_R^{-1} = CC^T(CC^T)^{-1} = I_{m\times m}, \tag{20}$$

where $I_{m\times m}$ is an $m \times m$ identity matrix. From the equations above, we know that matrix C_R^{-1} might work somehow like matrix C^{-1}. It is easy to obtain a particular solution of (10) as,

$$F = C_R^{-1}P. \tag{21}$$

To obtain all the solutions of (10), define two $n \times n$ matrices

$$\alpha = C_R^{-1}C = C^T(CC^T)^{-1}C, \tag{22}$$

$$\beta = I_{n\times n} - \alpha. \tag{23}$$

Some useful properties of the matrices α and β are listed as follows:

$$\text{rank}(\alpha) = m, \quad \text{rank}(\beta) = n - m, \quad C\alpha = C, \quad C\beta = 0, \quad \alpha^2 = \alpha, \quad \beta^2 = \beta, \quad \alpha\beta = 0. \tag{24}$$

Now the general solution of (10) can be presented as,

$$F = C_R^{-1}P + \beta X, \quad \forall X \in R^n. \tag{25}$$

For solving the linear compatibility equations of the system, presented in (13), we can consider a matrix whose number of rows is larger than the number of columns. Now from (13), C is still an $m \times n$ matrix with

$m < n$, while δ and D are vectors of dimension n and m, respectively. From the definition of the matrices α and β,

$$\alpha\delta = C^{\mathrm{T}}(CC^{\mathrm{T}})^{-1}CC^{\mathrm{T}}D = C^{\mathrm{T}}D = \delta, \quad \beta\delta = 0, \tag{26}$$

$$D = (CC^{\mathrm{T}})^{-1}C\delta = C_R^{-\mathrm{T}}\delta, \tag{27}$$

where $C_R^{-\mathrm{T}}$ represents the transpose of the generalized inverse C_R^{-1}.

In the next sections, this LIM formulation will be implemented to solve elastoplastic frame problems.

4. LIM formulation for elastoplastic frame element

The capabilities of the large increment method are extended, in the present section, to evaluate the nonlinear response of frame structures controlled by an elastic-fully plastic material model. The element forces are taken as the bending moment M, the shear force V and the normal force N that act at the centroid of the structural member at the far right end as shown in Fig. 2. The moment at any section along the beam can be given as:

$$M(x) = (x - L)V - M. \tag{28}$$

4.1. Yield function definition

Assuming that during elastic and plastic deformation, the cross-section remains planar and perpendicular to the neutral axis (i.e. Bernoulli hypothesis), the variation of strain in the member will be linear. Fig. 3 presents the strain and stress variations for a rectangular cross-sectional member of height h and width b for several stress levels.

The corresponding plastic hinge yield condition for this rectangular member in terms of axial force N and bending moment M can be written as,

$$\xi_{\mathrm{p}} - 1 = 0, \tag{29a}$$

where

$$\xi_{\mathrm{p}} = \left|\frac{M}{M_{\mathrm{p}}}\right| + \left(\frac{N}{N_{\mathrm{p}}}\right)^2 \tag{29b}$$

with M_{p} and N_{p} representing the maximum fully plastic moment and the maximum fully plastic normal force of the section, respectively. Thus,

$$M_{\mathrm{p}} = \frac{bh^2}{4}\sigma_{\mathrm{y}}, \quad N_{\mathrm{p}} = bh\sigma_{\mathrm{y}}. \tag{30}$$

This yield condition (29) can be illustrated by the two outer parabolas shown in Fig. 4.

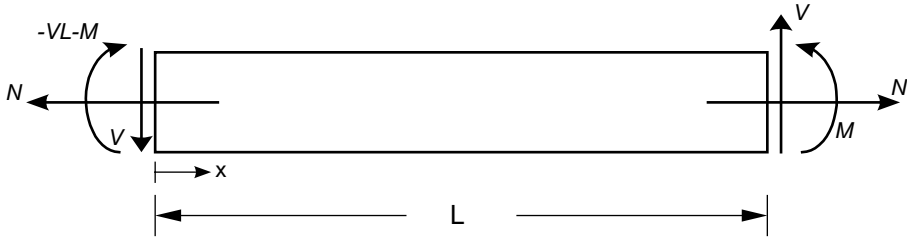

Fig. 2. Internal forces in frame element.

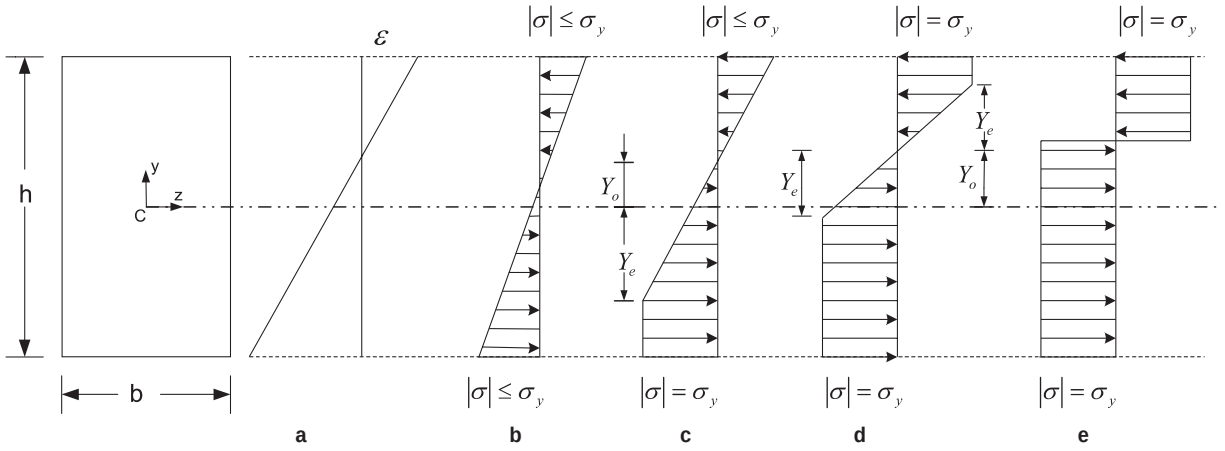

Fig. 3. Stress strain diagram for elastic and plastic cases; (a) strain diagram, (b) elastic stress diagram, (c,d) plastic stress diagram before plastic hinge formation and (e) plastic hinge stress case (i.e. fully plastic section).

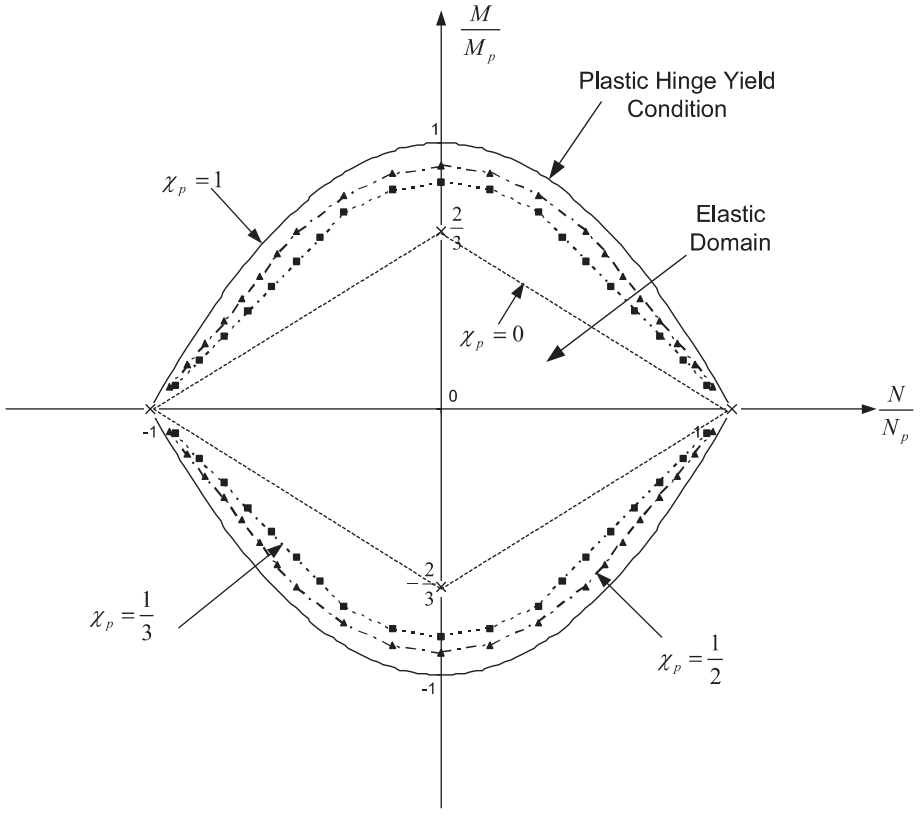

Fig. 4. Yield condition.

The domain of the purely elastic state of the rectangular member is also indicated in the figure by the inner dashed lines defined by the equation,

$$\xi_e - 1 = 0, \tag{31a}$$

where

$$\xi_e = \left|\frac{M}{M_e}\right| + \left|\frac{N}{N_e}\right| \tag{31b}$$

with M_e and N_e as the maximum fully elastic moment and the maximum fully elastic normal force of the section, respectively. Consequently,

$$M_e = \frac{bh^2}{6}\sigma_y, \quad N_e = bh\sigma_y. \tag{32}$$

Transitional behavior can be characterized in terms of a non-dimensional parameter χ_p, representing the fraction of the cross-section at the yield stress. Thus $\chi_p = 0$ for the elastic case (Fig. 3b), while $\chi_p = 1$ for the case of a plastic hinge (Fig. 3e). The curves for several intermediate values of χ_p are shown in Fig. 4, along with the two limiting cases.

4.2. Stress functions formulation

For each element, the stress at any point along the element length and depth can be written in terms of element forces (N, V, M) such that,

$$\sigma(x,y) = Z_1(x,y)N + Z_2(x,y)V + Z_3(x,y)M, \tag{33}$$

where Z_1, Z_2, Z_3 are the stress shape functions. The stress and stress shape functions for the different regimes that are presented in Fig. 3 can be written in the following forms.

Case 1: Elastic (Fig. 3b)

The elastic stress through the depth of the cross-section can be easily derived and can be defined by,

$$\sigma(x,y) = \frac{N}{A} + \frac{M(x)y}{I} = \frac{N}{A} + \frac{(x-L)y}{I}V - \frac{y}{I}M. \tag{34}$$

Thus,

$$Z_1(x,y) = \frac{1}{A}, \quad Z_2(x,y) = \frac{(x-L)y}{I}, \quad Z_3(x,y) = -\frac{y}{I}. \tag{35}$$

Case 2: Elastoplastic (Fig. 3c)

In this case, two regions can be distinguished; the linear variation of stress through the depth of the cross-section and the constant stress variation. In the linear part, the stress can be written in the following form:

$$\sigma = \left(\frac{y - Y_0}{Y_0 + Y_e}\right)\sigma_y. \tag{36}$$

By adding and subtracting N/A and then pre-multiply by $M(x)/M(x)$, one can obtain,

$$\sigma = \left[\eta\sigma_y - \frac{N}{A}\right]\frac{(x-L)V - M}{(x-L)V - M} + \frac{N}{A} \tag{37}$$

with the non-dimensional parameter $\eta = (y - Y_0)/(Y_0 + Y_e)$. Thus,

$$Z_1(x,y) = \frac{1}{A},$$
$$Z_2(x,y) = \frac{\left[\eta\sigma_y - \frac{N}{A}\right](x-L)}{[(x-L)V + M]}, \tag{38}$$
$$Z_3(x,y) = -\frac{\left[\eta\sigma_y - \frac{N}{A}\right]}{[(x-L)V + M]}.$$

On the other hand, the stress on the constant stress region can be defined as,

$$\sigma = -\sigma_y. \tag{39}$$

The expressions (37) and (38) remain valid, but now with $\eta = -1$.

Case 3: Elastoplastic (Fig. 3d)

In this case, three regions can be recognized; the lower constant variation through the depth, the central linear variation and the upper constant variation. The corresponding stress in the three regions can be expressed as in (37) with $\eta = -1$, $\eta = (y - Y_0)/Y_e$ and $\eta = +1$, respectively. The stress shape functions are written as in (38) for each region.

Case 4: Fully plastic (Fig. 3e)

For the case of the plastic hinge, let $\eta = -1$ and $\eta = +1$ for the lower and upper constant stress regions, respectively. Then, once again, the stress is defined by (37) and the stress shape functions are given by (38).

For all loading states, the regions associated with the three stress phases (i.e. elastic, elastoplastic, plastic) presented in Fig. 3 can be easily distinguished through the element length and the linear strain variation through the element depth can be determined for each region.

4.3. Local element deformations

Knowing the moment distribution and axial force along the element length, it is possible to divide the member into elastic regions (i.e. $\xi_e < 1$), and plastic regions (i.e. $\xi_e \geqslant 1$). The element deformations are functions of the stress shape functions and the strain along the beam. Therefore, the deformations can be written as,

$$\delta_i = \int Z_i(x,y)\varepsilon(x,y)\,d\Omega, \quad i = 1,2,3. \tag{40}$$

In each iteration, these relations give the deformations for each element as a result of the internal force vector in that iteration. These deformations are not necessarily sufficiently compatible with the deformations of the other elements, and therefore an iterative procedure is needed to achieve convergence.

4.4. Plastic hinge representation

As was mentioned before, as the loads are increased, plastic hinges may begin to form at the element ends and (29a) then applies at different locations on the structure. The developed plastic hinge is represented by the tangent of the point on the yield surface as shown in Fig. 5. Point A, in the figure, is an assumed plastic hinge with $\overline{N}$ and $\overline{M}$ as the internal forces, such that,

$$\left|\frac{\overline{M}}{M_p}\right| + \left(\frac{\overline{N}}{N_p}\right)^2 = 1. \tag{41}$$

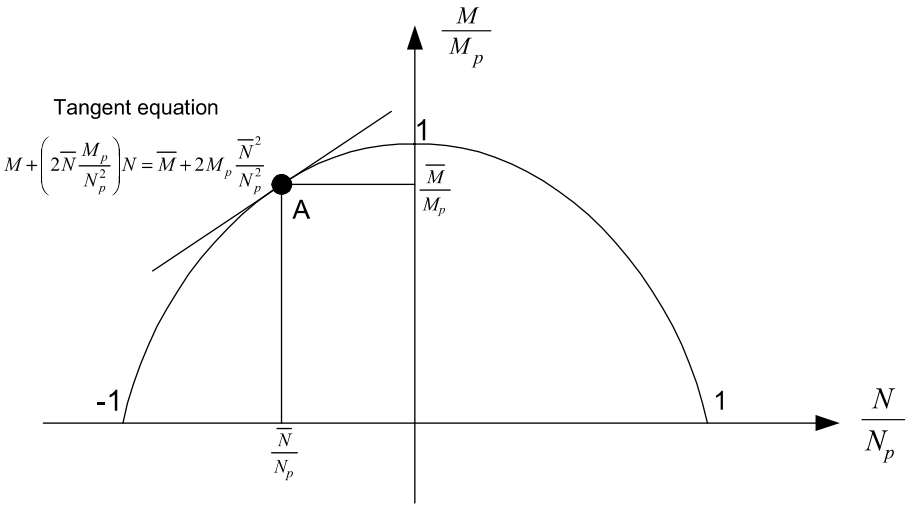

Fig. 5. Plastic hinge representation.

Then the slope of the tangent line at A can be given by,

$$\frac{\mathrm{d}M}{\mathrm{d}N} = -2\overline{N}\frac{M_{\mathrm{p}}}{N_{\mathrm{p}}^2}. \tag{42}$$

Thus, the tangent equation at point A can be written as,

$$M + \left(2\overline{N}\frac{M_{\mathrm{p}}}{N_{\mathrm{p}}^2}\right)N = \overline{M} + 2M_{\mathrm{p}}\frac{\overline{N}^2}{N_{\mathrm{p}}^2}. \tag{43}$$

With the formation of a plastic hinge, the relationship (43) is incorporated in the equilibrium equations in (10) by adding an extra row to the equilibrium matrix C and a corresponding component to generalized load vector P. This tangent equation will allow the hinge to slide slightly along the tangent direction in generalized force space, as indicated in Fig. 5. The tangent equation can be modified when point A moves outside the yield surface as will be described later in the discussion of the return algorithm.

In addition to (43), we also must enforce kinematic coupling between plastic hinge rotation and the member axial extension, because the rotation is not necessarily about the neutral axis. To explain this, consider Fig. 6 below. For the most general case of combined bending and axial load, the relation between plastic hinge rotation θ_{p} and axial extension δ_{axial} can be written,

$$\frac{1}{2}(2\zeta - 1)h\theta_{\mathrm{p}} = \delta_{\mathrm{axial}}. \tag{44}$$

In terms of generalized forces, this becomes

$$2\overline{N}\frac{M_{\mathrm{p}}}{(N_{\mathrm{p}})^2}\theta_{\mathrm{p}} = \delta_{\mathrm{axial}}. \tag{45}$$

Interestingly, (45) can be enforced within the present framework simply by adding an extra variable θ_{p} to the generalized nodal free displacement vector D and then using the new row–augmented C matrix, defined above, within the overall system compatibility Eq. (13). Thus, the generalized force–displacement duality is extended to encompass the behavior of plastic hinges.

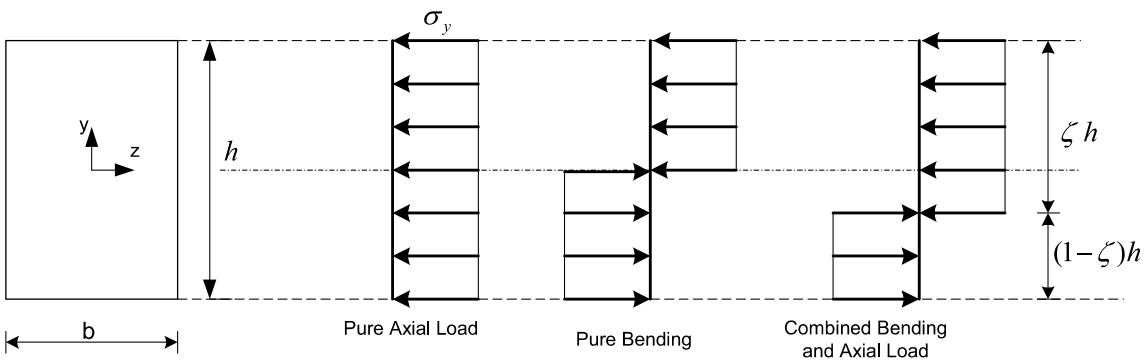

Fig. 6. Plastic hinge case.

5. Solution procedure

5.1. Overview

The flow chart in Fig. 7 provides an overview of the entire LIM solution procedure. The first step in the large increment method is to obtain an initial force vector that satisfies the equilibrium equations. For frame structures controlled by an elastic fully plastic material model, all elements end forces must satisfy $\xi_p \leqslant 1$. In other words, the element end forces must lie on or inside the plastic hinge surface. For this reason a return algorithm might be needed for the points which are found to be outside the hinge surface when using the generalized inverse to solve (10). (Details are provided in Section 5.3.) Thereafter, the force vector resulting from this step is used in the local stage to compute the element deformations that are controlled by the nonlinear constitutive material model. This nonlinear local stage requires the formation of the element-based tangent flexibility matrix ϕ' and stiffness matrix κ' to determine appropriate search directions. However, for elements containing one or more plastic hinges, these operations must be performed with care, as described subsequently in Section 5.2. We note here that in any case this nonlinear local stage can be done in a parallel computing platform for each element separately. After that the compatibility condition defined in (26) is used to check whether the deformations are compatible or not. If not, the error in the deformations resulting from the compatibility equations is employed to calculate a more accurate force vector in an iterative technique. The algorithm automatically decides whether or not a plastic hinge is formed at any location in the structure.

5.2. Flexibility coefficients

The flexibility coefficients will be calculated as proposed by Barham et al. (2003) where for a plastic member, the flexibility coefficient calculations are based on the part that remains elastic. The plastic part has no contribution to the flexibility matrix for elastic-perfectly plastic constitutive models. Consequently, the flexibility coefficients approach to infinity for any element that has a plastic hinge in one or both of its ends. To overcome this singularity, a spectral decomposition approach is developed. Whenever a plastic

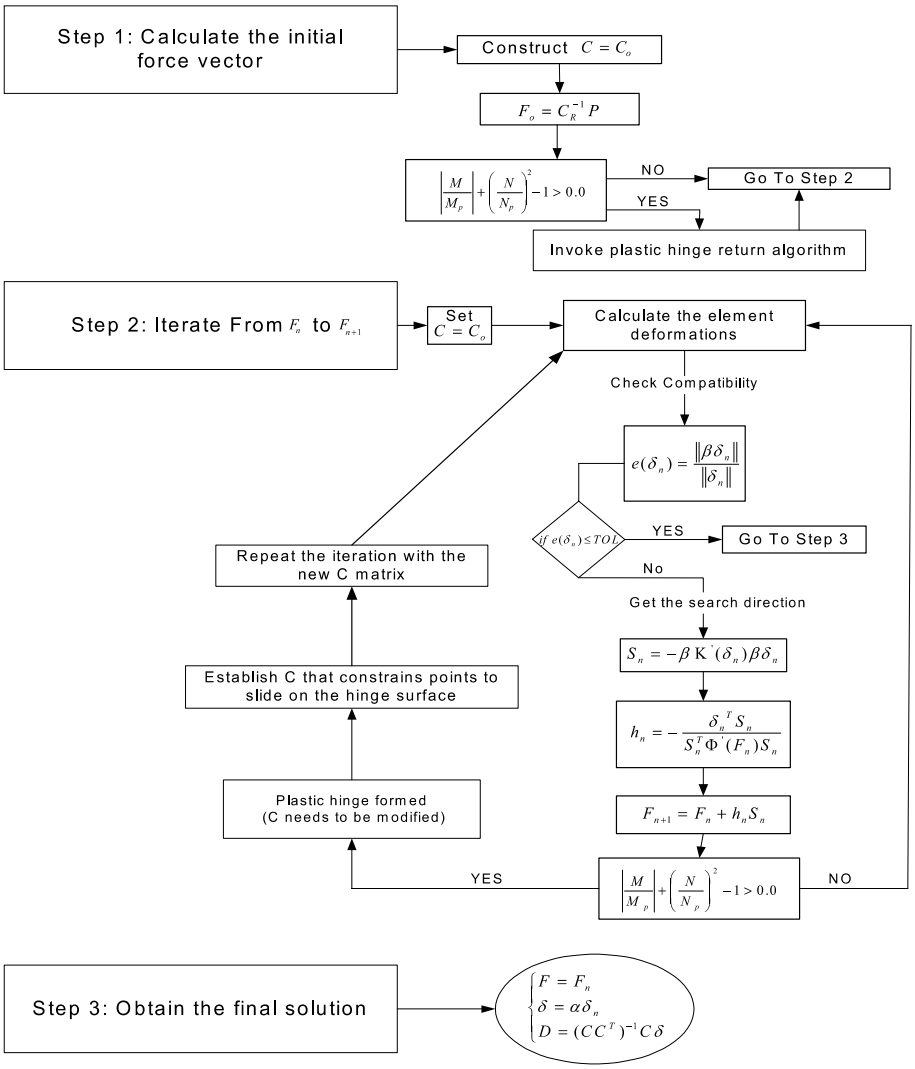

Fig. 7. Solution procedure.

hinge forms, the flexibility eigenvalue corresponding to the rotation mode goes to infinity. This in turn will cause all the flexibility coefficients to approach infinity. However, by isolating this mode it is possible to generate a finite reduced flexibility matrix and a corresponding finite reduced stiffness matrix that can be used in the LIM algorithm.

We begin by writing the element flexibility matrix in spectral form as,

$$\phi' = \frac{\partial \varphi}{\partial F} = \Theta^{\mathrm{T}} \lambda \Theta \tag{46}$$

with diagonal eigenvalue matrix λ and eigenvectors Θ. In the planar frame problem, we have three modes. Only the rotational eigenvalue goes to infinity when a plastic hinge is formed. However, this has no contribution to the element stiffness. By removing this mode, it is possible to generate a reduced flexibility ma-

trix and a reduced stiffness matrix from the reduced diagonal eigenvalue matrices λ_{reduced} and $\lambda^{-1}_{\text{reduced}}$, which both have zero value for the rotational eigenvalue. Then it is possible to write,

$$\phi'_{\text{reduced}} = \Theta^{\text{T}} \lambda_{\text{reduced}} \Theta. \tag{47}$$

Once the element flexibility matrix is determined, the stiffness matrix can be calculated separately for each element. This is a computationally low cost process since it requires only an inverse of a 3×3 flexibility matrix for the elements with no plastic hinges. For the elements with one or two plastic hinges, the simple spectral decomposition is utilized, as described above. Then, the corresponding element stiffness matrix becomes,

$$\kappa'_{\text{reduced}} = \Theta^{\text{T}} \lambda^{-1}_{\text{reduced}} \Theta. \tag{48}$$

In the LIM solution procedure shown in Fig. 7, the global flexibility and stiffness matrices Φ' and K', respectively, are required to establish the search direction S_n and step size h_n for iteration n. Notice, however, that Φ' and K' involve no coupling between elements. These global flexibility and stiffness matrices can be written as,

$$\Phi' = \begin{bmatrix} \phi'_{e_1} & & & \\ & \phi'_{e_2} & & \\ & & \cdots & \\ & & & \phi'_{e_\rho} \end{bmatrix}, \tag{49}$$

$$K' = \begin{bmatrix} \kappa'_{e_1} & & & \\ & \kappa'_{e_2} & & \\ & & \cdots & \\ & & & \kappa'_{e_\rho} \end{bmatrix}. \tag{50}$$

5.3. Return algorithm

The goal of the return algorithm is to enforce all the element end forces to be in the acceptable range (i.e. on or inside the parabolic hinge surface). The generalized inverse from (10) will produce a force vector that is in equilibrium but some end forces may be outside the hinge surface. However, in order to start the LIM iterations, all points must lie on or inside the plastic hinge surface. Consequently, a return procedure is proposed here and shown in detail in a flow chart form in Fig. 8. The return algorithm begins with the elastic solution for the applied loading, which can be obtained as described in Appendix A. If the elastic solution lies on or inside the hinge surface, then these forces will be adopted as the initial internal element forces for LIM iterations. For high levels of loading some of the element end forces might lie outside the hinge surface, and for this case the return algorithm is needed.

For the present implementation, the equilibrium matrix C will be modified by a number of linear equations equal to the degree of indeterminacy (l) of the structural system. After arranging, the element end forces in descending order according to ξ_{p}, the first (l) ends will be chosen to be added to the equilibrium matrix C. Some of these lines will be tangent to the hinge surface which represent group 1. The rest are passed though the hinge surface center which represent group 2 as initial directional equations.

If more than one step is needed to reach to the solution for the entire load (i.e. $\mu < 1$), then after solving for μP using the LIM algorithm, the element end forces will be arranged again based on ξ_{p} values. Thus, changes in membership might take place to group 1, group 2 and group 3. The directional lines equations representing group 2 will take into account the plastic solution of the previous steps as shown in Fig. 9. The algorithm continues until we solve for the entire loading path or until the number of plastic hinges formed is equal to the degree of indeterminacy of the system. At that point the collapse load is reached; no more equations can be added to represent new plastic hinges since we will have an unstable structure.

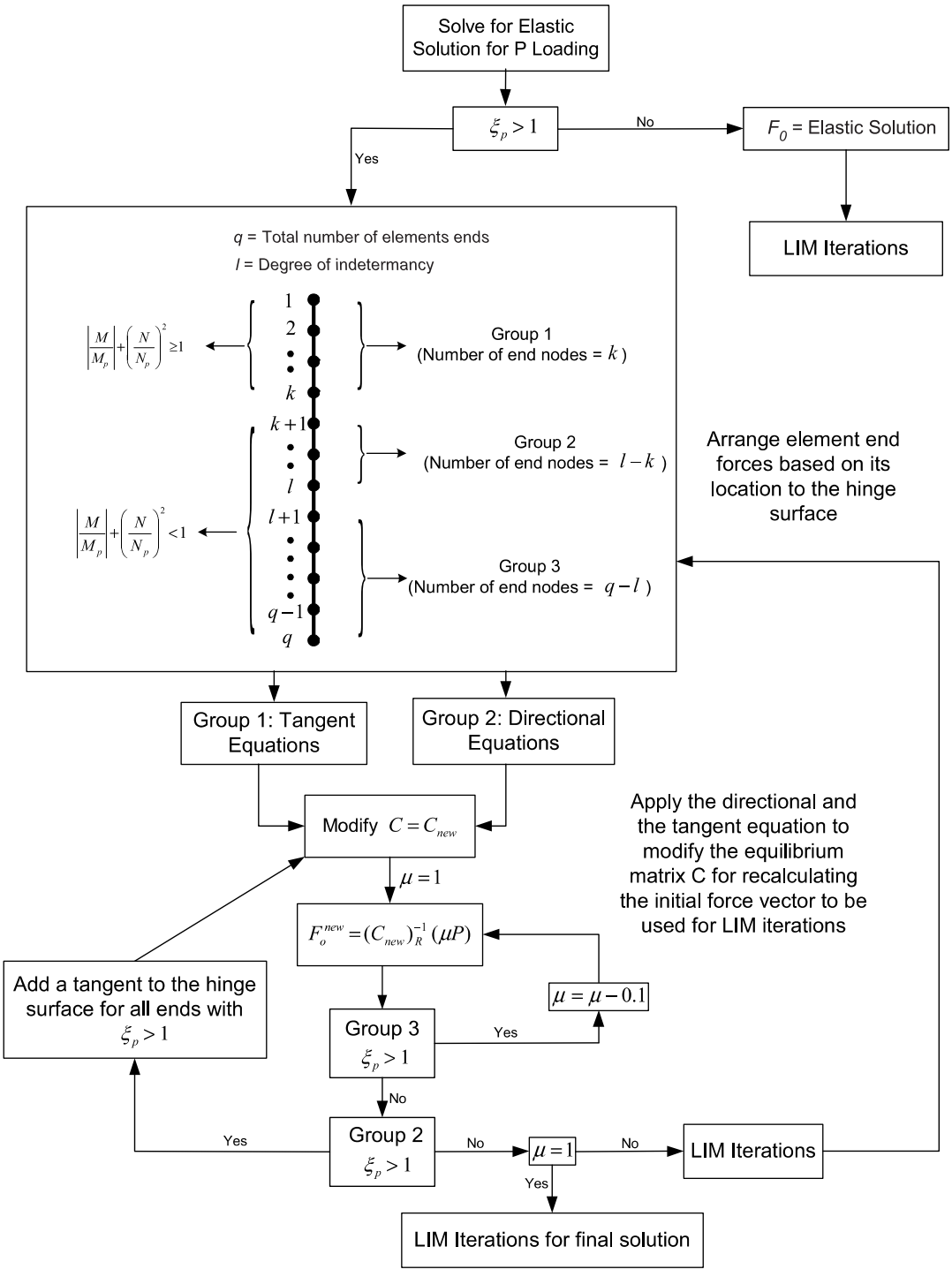

Fig. 8. Return algorithm.

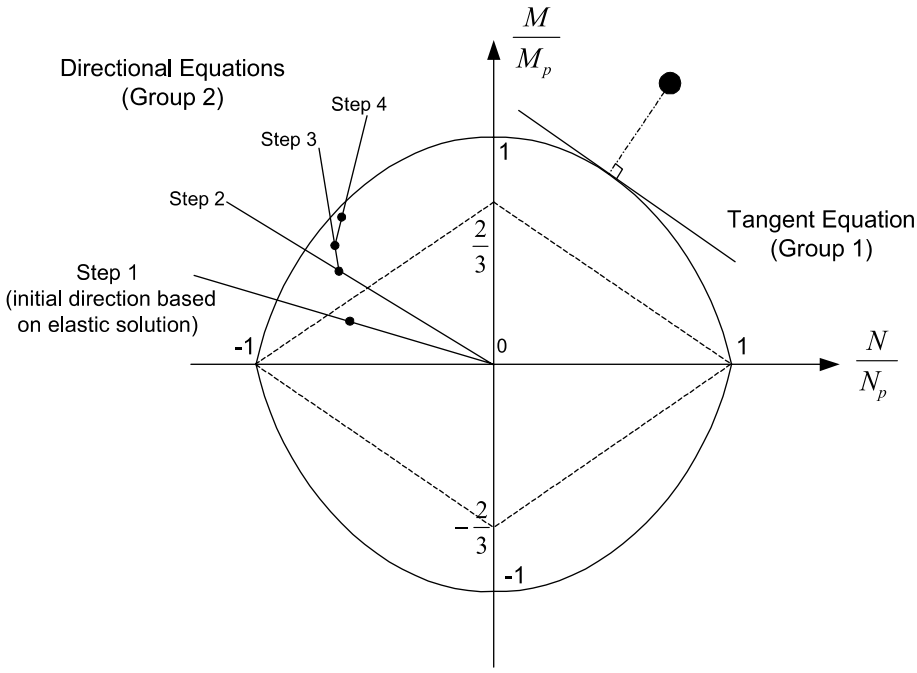

Fig. 9. Tangent and directional equations.

6. Numerical examples

In this section, two examples will be presented. The problems will be solved by the LIM approach and the finite element program ABAQUS (2003), which utilizes the displacement method.

Example 1. Consider the following staircase frame structure shown in Fig. 10. The constitutive relation that governs the behavior of the structure is also presented in the same figure. The structure will be loaded

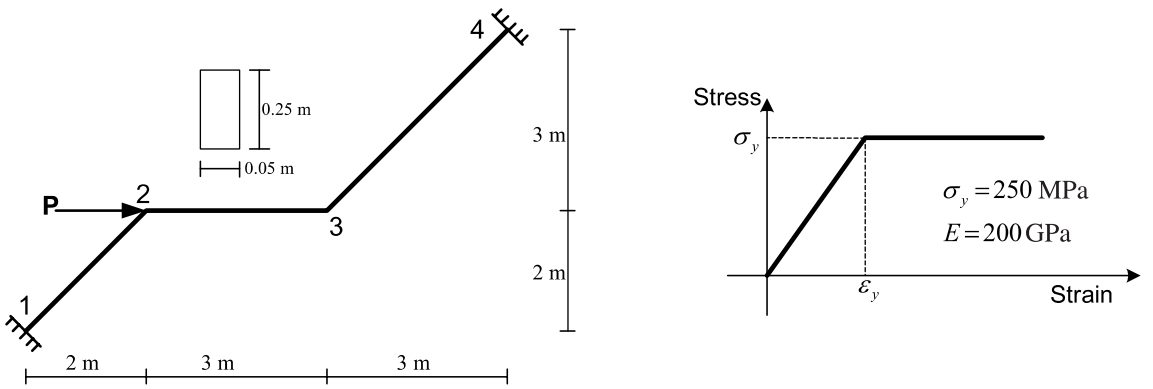

Fig. 10. Geometry of the staircase frame problem.

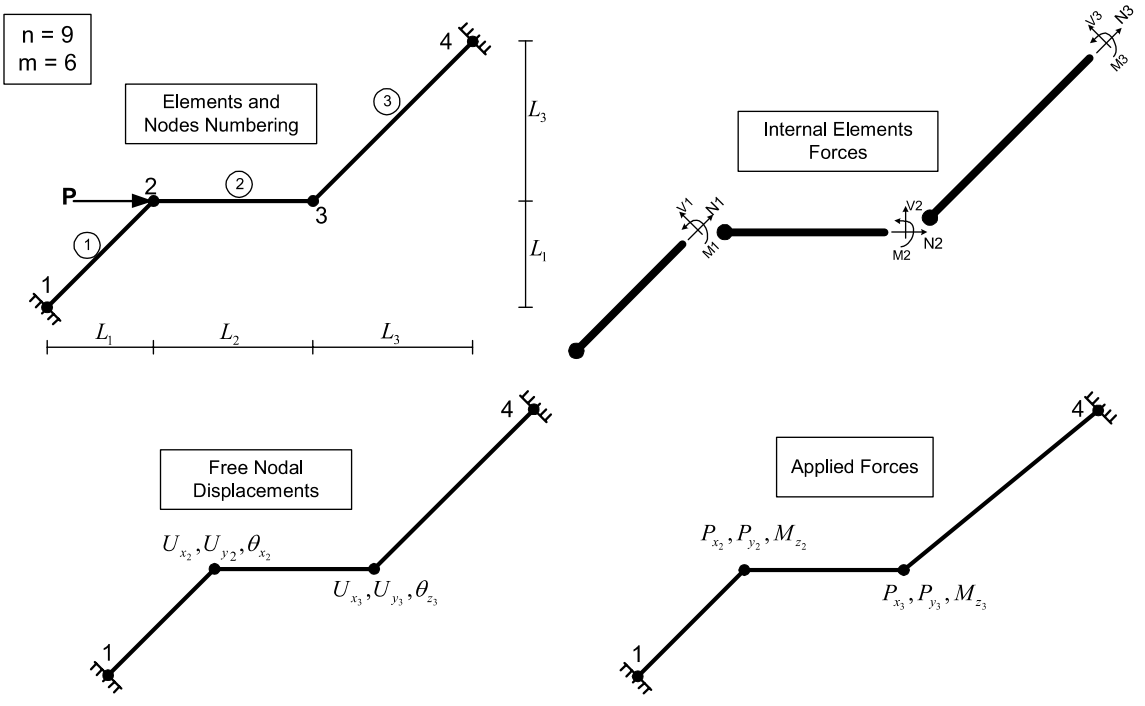

$$F = \begin{Bmatrix} N1 \\ V1 \\ M1 \\ N2 \\ V2 \\ M2 \\ N3 \\ V3 \\ M3 \end{Bmatrix} \qquad P = \begin{Bmatrix} P_{x_2} \\ P_{x_2} \\ M_{z_2} \\ P_{x_3} \\ P_{y_3} \\ M_{z_3} \end{Bmatrix}$$

$$\begin{bmatrix} \frac{\sqrt{2}}{2} & -\frac{\sqrt{2}}{2} & 0 & -1 & 0 & 0 & 0 & 0 & 0 \\ \frac{\sqrt{2}}{2} & \frac{\sqrt{2}}{2} & 0 & 0 & -1 & 0 & 0 & 0 & 0 \\ 0 & 0 & 1 & 0 & -L_2 & -1 & 0 & 0 & 0 \\ 0 & 0 & 0 & 1 & 0 & 0 & -\frac{\sqrt{2}}{2} & \frac{\sqrt{2}}{2} & 0 \\ 0 & 0 & 0 & 0 & 1 & 0 & -\frac{\sqrt{2}}{2} & -\frac{\sqrt{2}}{2} & 0 \\ 0 & 0 & 0 & 0 & 0 & 1 & 0 & -\sqrt{2}L_3 & -1 \end{bmatrix} \begin{Bmatrix} N1 \\ V1 \\ M1 \\ N2 \\ V2 \\ M2 \\ N3 \\ V3 \\ M3 \end{Bmatrix} = \begin{Bmatrix} P_{x_2} \\ P_{y_2} \\ M_{z_2} \\ P_{x_3} \\ P_{y_3} \\ M_{z_3} \end{Bmatrix}$$

$$\delta = \begin{Bmatrix} \delta_{u1} \\ \delta_{v1} \\ \delta_{\theta 1} \\ \delta_{u2} \\ \delta_{v2} \\ \delta_{\theta 2} \\ \delta_{u3} \\ \delta_{v3} \\ \delta_{\theta 3} \end{Bmatrix} \qquad D = \begin{Bmatrix} U_{x_2} \\ U_{y_2} \\ \theta_{z_2} \\ U_{x_3} \\ U_{x_3} \\ \theta_{z_3} \end{Bmatrix}$$

$$\begin{bmatrix} \frac{\sqrt{2}}{2} & \frac{\sqrt{2}}{2} & 0 & 0 & 0 & 0 \\ -\frac{\sqrt{2}}{2} & \frac{\sqrt{2}}{2} & 0 & 0 & 0 & 0 \\ 0 & 0 & 1 & 0 & 0 & 0 \\ -1 & 0 & 0 & 1 & 0 & 0 \\ 0 & -1 & -L_2 & 0 & 1 & 0 \\ 0 & 0 & -1 & 0 & 0 & 1 \\ 0 & 0 & 0 & -\frac{\sqrt{2}}{2} & -\frac{\sqrt{2}}{2} & 0 \\ 0 & 0 & 0 & \frac{\sqrt{2}}{2} & -\frac{\sqrt{2}}{2} & -\sqrt{2}L_2 \\ 0 & 0 & 0 & 0 & 0 & -1 \end{bmatrix} \begin{Bmatrix} \delta_{u1} \\ \delta_{v1} \\ \delta_{\theta 1} \\ \delta_{u2} \\ \delta_{v2} \\ \delta_{\theta 2} \\ \delta_{u3} \\ \delta_{v3} \\ \delta_{\theta 3} \end{Bmatrix} = \begin{Bmatrix} U_{x_2} \\ U_{y_2} \\ \theta_{z_2} \\ U_{x_3} \\ U_{x_3} \\ \theta_{z_3} \end{Bmatrix}$$

Fig. 11. Staircase frame primary analysis.

up to the failure point. Only three elements were used in the LIM analysis with exact integration along the element length and depth. On the other hand, in order to capture the true behavior of the structure, we used a total of 202 evenly spaced B23 beam elements from the ABAQUS library to build the finite element mesh.

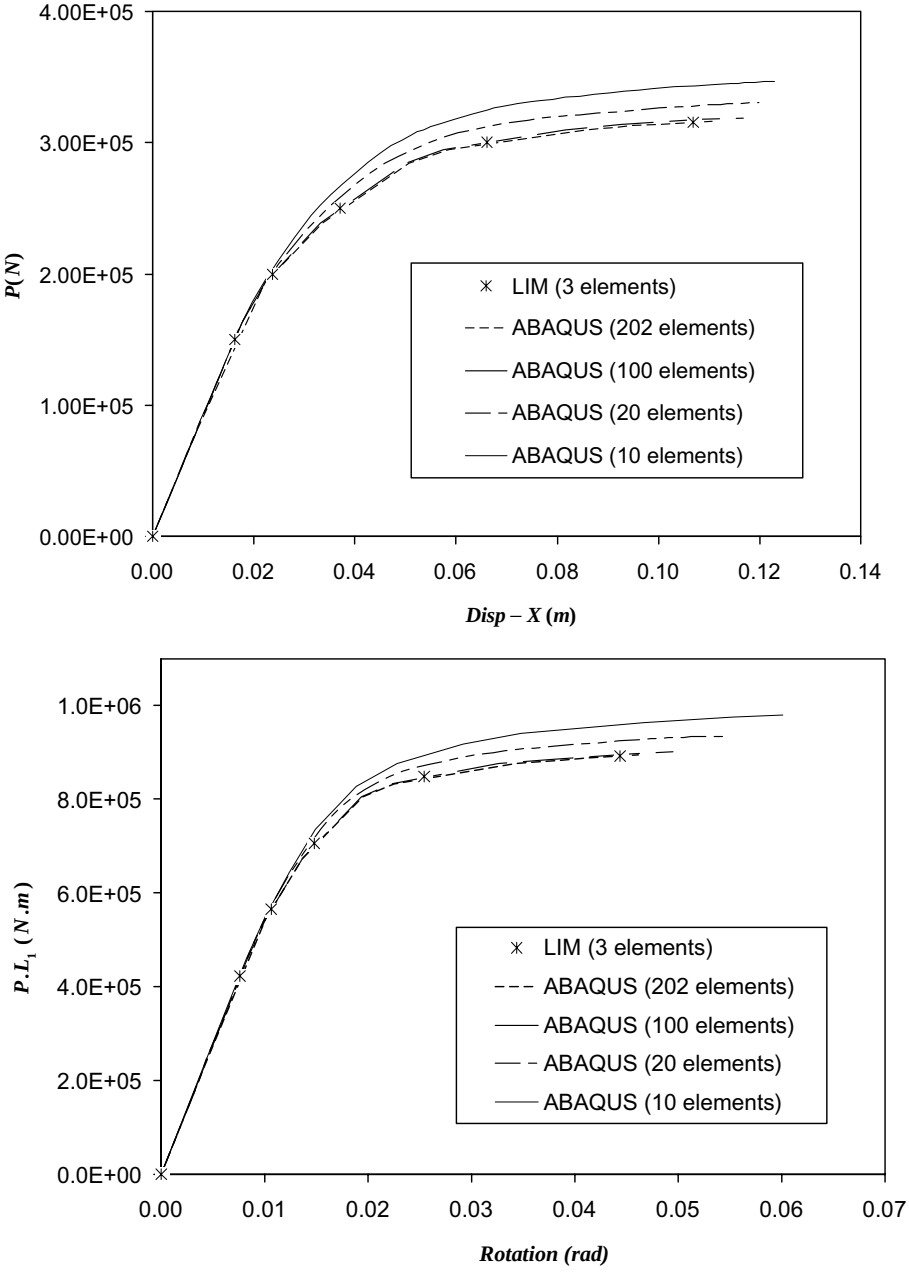

Fig. 12. Comparison of LIM with ABAQUS for staircase frame.

A large number of integration points (25 integration points) were employed through the beam depth in the ABAQUS analysis in order to obtain accurate results and capture the collapse load.

To gain better understanding for the present force-based approach, consider Fig. 11, which presents a primary analysis for this frame problem. Three internal element forces and three local deformations are defined for each of the three elements. Thus $n = 9$. While the dimension of the applied force vector and the nodal displacement vector is 6 (i.e. $m = 6$). Details for the F, P, δ and D vectors are provided in the figure, along with the components of the equilibrium matrix C.

Fig. 12 presents a comparison between LIM and ABAQUS results for the horizontal displacement and rotation versus P for the node 2 under the load. A convergence study for the ABAQUS solutions is also included in the figure. Clearly, with increasing mesh refinement, ABAQUS results approach the LIM solution.

Fig. 13 follows the evolution of yield in the elastic–plastic regime for the two supports points, labeled 1 and 4. The increase in the plasticity index ξ_p is recorded and plotted at each step in the loading path.

In order to have better understanding about the flexibility analysis, Fig. 14 is introduced. Here, the eigenvalues and eigenvectors are presented for element 1 for both the elastic state and after the formation of a plastic hinge. In the latter case, the rotational eigenvalue tends to infinity. According to our algorithm presented in Section 5.2, this third mode was omitted from the flexibility and stiffness calculation in (47) and (48) by forming λ_{reduced}.

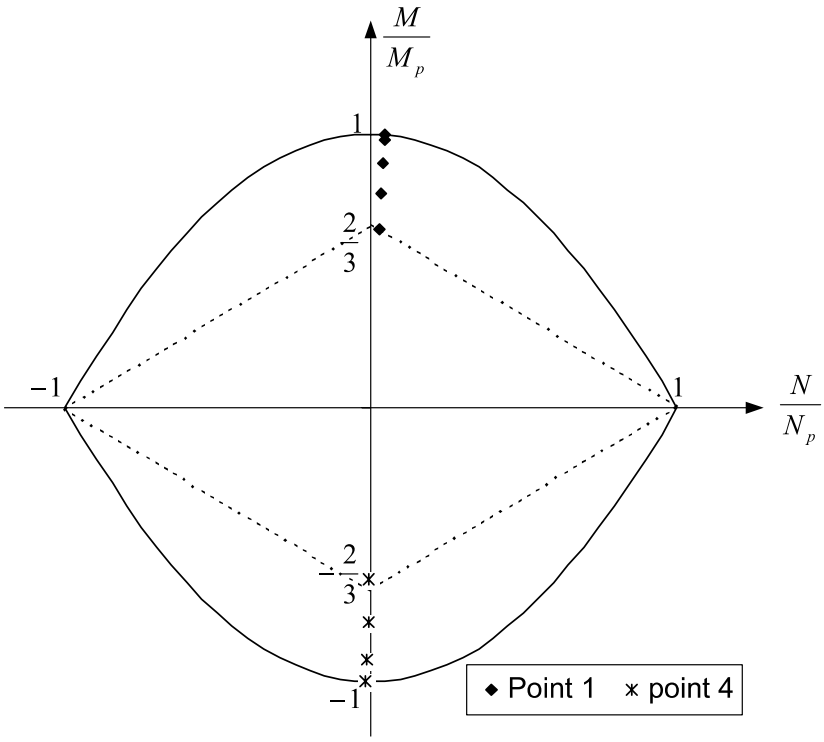

Fig. 13. Plasticity evolution at points 1 and 4 for staircase frame.

Elastic flexibility matrix of element 1

$$\phi_e' = \Theta_e^T \lambda_e \Theta_e$$

Elastic stiffness matrix of element 1

$$k_e' = \Theta_e^T \lambda_e^{-1} \Theta_e$$

Eigenvalues

$$\lambda_e = \begin{bmatrix} 0.1131\text{e-}8 & 0 & 0 \\ & 0.4172\text{e-}7 & 0 \\ 0 & 0 & 0.7548\text{e-}6 \end{bmatrix}$$

Eigenvectors

$$\Theta_e = \begin{bmatrix} 1 & 0 & 0 \\ 0 & -0.4961 & 0.8682 \\ 0 & 0.8682 & 0.4961 \end{bmatrix}$$

Flexibility matrix of element 1 with plastic hinge at the left end

$$\phi_{Ph}' = \Theta_{Ph}^T \lambda_{reduced} \Theta_{Ph} \qquad Ph: Plastic\ hinge$$

Stiffness matrix of element 1 with plastic hinge at the left end

$$k_{Ph}' = \Theta_{Ph}^T \lambda_{reduced}^{-1} \Theta_{Ph}$$

Eigenvalues

$$\lambda_{Ph} = \begin{bmatrix} 0.1352\text{e-}8 & 0 & 0 \\ & 0.6832\text{e-}7 & 0 \\ 0 & 0 & \infty \end{bmatrix}$$

Reduced eigenvalues

$$\Rightarrow \lambda_{reduced} = \begin{bmatrix} 0.1352\text{e-}8 & 0 & 0 \\ & 0.6832\text{e-}7 & 0 \\ 0 & 0 & 0 \end{bmatrix}$$

Eigenvectors

$$\Theta_{Ph} = \begin{bmatrix} 1 & 0 & 0 \\ 0 & -0.3333 & 0.9428 \\ 0 & 0.9428 & 0.3333 \end{bmatrix}$$

Fig. 14. Sample flexibility and stiffness analysis for staircase frame.

Finally, a quantitative comparison between LIM and the displacement-based FE approach is presented in Table 1 for point 2, which includes the number of iterations needed in both approaches. Notice that the proposed LIM algorithm requires only three elements to achieve excellent results, even as the collapse load is approached.

Table 1
Comparison of LIM with ABAQUS for staircase frame (point 2)

P (N)	ABAQUS (202 elements)			LIM (3 elements)		
	Disp-X (m)	Rotation (rad)	Iterations	Disp-X (m)	Rotation (rad)	Iterations
1.5e5	0.016273	0.007621	4	0.016271	0.007623	4
2.0e5	0.023671	0.010579	5	0.023694	0.010574	6
2.5e5	0.036754	0.014703	23	0.037101	0.014771	17
3.0e5	0.065386	0.025351	30	0.066709	0.026170	22

Example 2. In this example, a two-story frame structure will be considered. The geometry and the constitutive relation are shown in Fig. 15. In the LIM analysis, only six elements were used with exact integration along the element length and through the cross-section depth. Meanwhile, in the ABAQUS solution, we used an element length of 0.025 m with a total number of 720 B23 elements from the ABAQUS library. A total number of 25 integration points within the element depth were employed in the FE analysis. The structure is subjected to external applied loads as shown in the figure below.

Fig. 16 shows the horizontal and vertical displacement of node 2 versus P in addition to the rotation of the hinge (node 6) versus PL_1. LIM solutions are included, along with a study of ABAQUS solutions. Quantitative results are presented in Table 2 for points 2 and 6 for both ABAQUS and LIM. The corresponding number of iterations is also included.

6.1. Discussion

It is obvious from Figs. 12 and 16 that the ABAQUS solution converges to the LIM solution as the FE mesh become finer and more elements are used to represent the structure. This occurs because in LIM we utilize an element that exactly represents the plastic behavior of a Bernoulli elastoplastic frame element. This LIM element employs exact stress shape functions and exact integration.

Tables 1 and 2 compare the number of iterations needed to reach the solution using LIM and ABAQUS. From the tables, the efficiency of both methods in terms of iterations to convergence tends to be similar at low levels of loading. That is the case for the first two rows of Tables 1 and 2, where in both cases there was

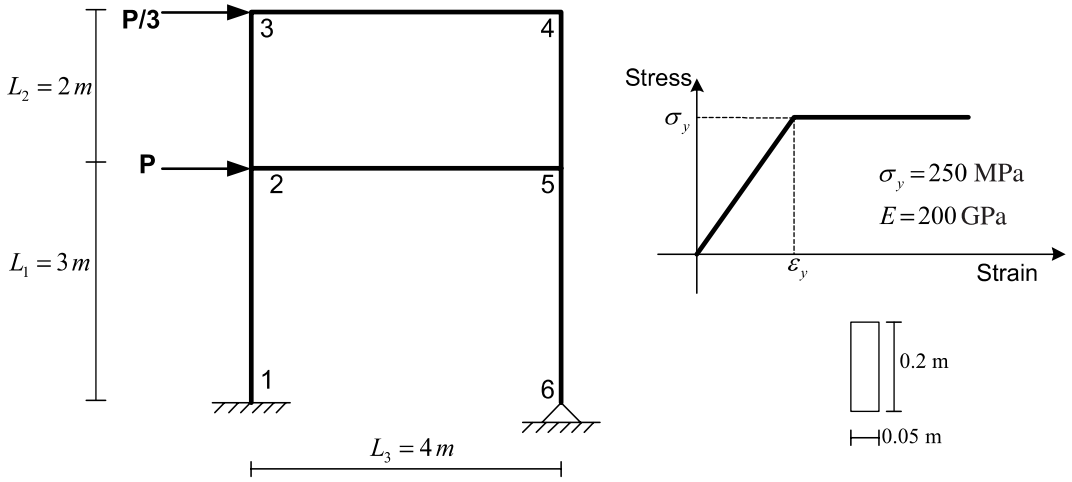

Fig. 15. Geometry of the two story frame problem.

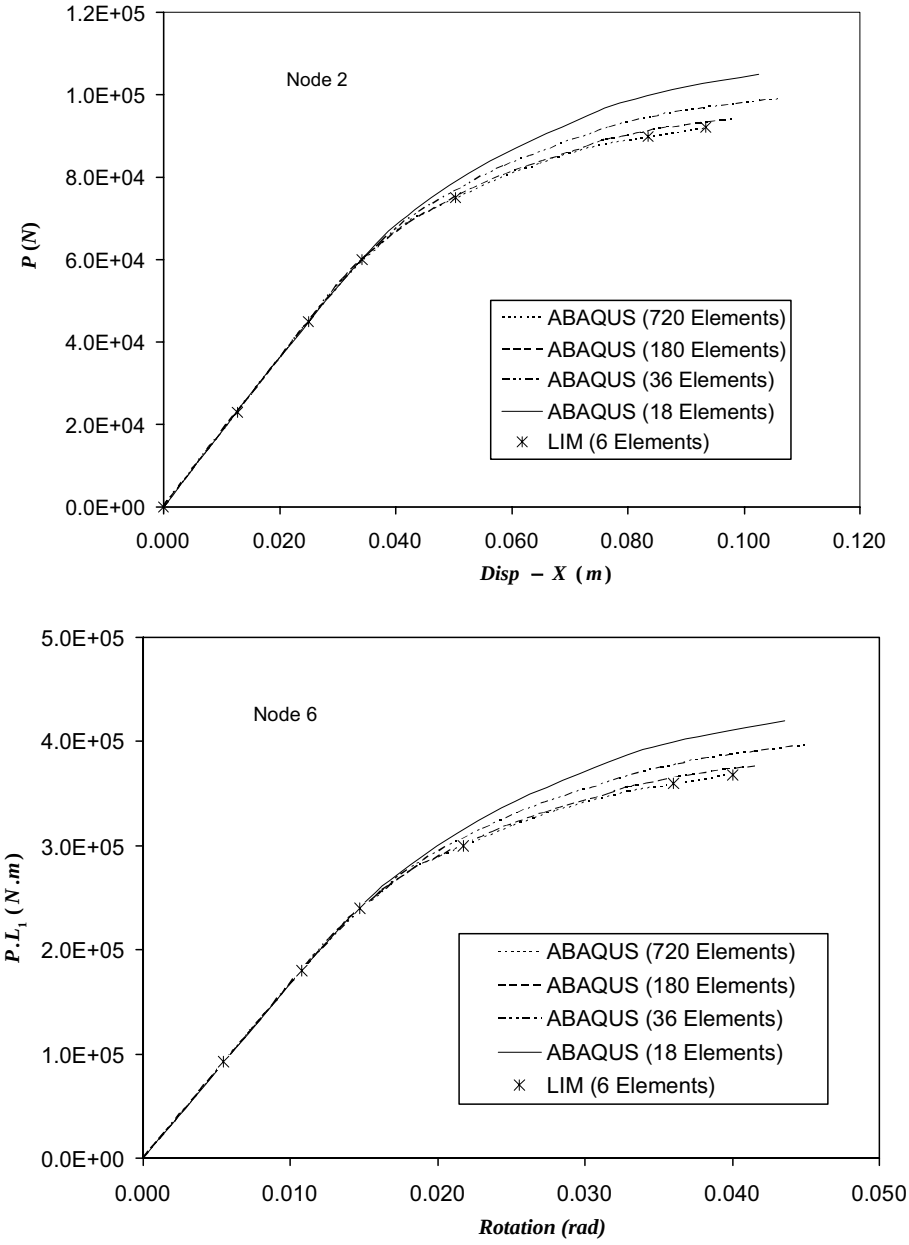

Fig. 16. Comparison of LIM with ABAQUS for two-story frame (point 2).

no plastic hinge formation. After that, plastic hinges start to form in the structure (nodes 1, 2 and 4) in Example 1 and (nodes 1 and 2) in Example 2. With the formation of the plastic hinges, LIM performance appears to be superior to ABAQUS, as the difference in the number of iterations needed to reach the solution in the two methods becomes significant. In both methods more than one step was needed to solve the examples for high levels of loading, when plasticity spread more in the structure. However, the permissible LIM load step is larger than the acceptable ABAQUS step.

Table 2
Comparison of LIM iterations with ABAQUS iterations for two-story frame

P (N)	ABAQUS (720 elements)			LIM (6 elements)		
	Disp-X (m) (point 2)	Rotation (point 6)	Number of iterations	Disp-X (m) (point 2)	Rotation (point 6)	Number of iterations
4.5e4	0.02497	0.01075	5	0.02493	0.01073	7
6.0e4	0.034219	0.01474	5	0.03416	0.01471	6
7.5e4	0.050373	0.021787	16	0.05054	0.021869	14
9.0e4	0.083612	0.036106	48	0.08421	0.03648	25

Consequently, LIM can be viewed as a very efficient computational algorithm compared to the traditional displacement method, since LIM needs a minimal number of elements to represent the structural system while permitting the use of large load increments.

7. Conclusions

This paper presents the extension of the large increment methodology for the nonlinear analysis of plane frame structures controlled by an elastic, perfectly plastic material model. The LIM iterative procedure was able to handle the complexity of this problem for the illustrative examples. One of the main advantages of LIM is that it can reach the solution with very few numbers of elements and load increments, unlike the displacement-based method. The efficiency of LIM strongly appears when the plastic hinges start to form in the structure and the structure approaches the collapse load. However, additional research is needed to extend this analysis approach to cover other important nonlinear problems (e.g., cyclic loading analysis, geometric nonlinearity).

Acknowledgments

This research was funded by the National Science Foundation, grant number CMS-0002936 with Dr. Vijaya Gopu as program director. The authors gratefully acknowledge this support. The results obtained express the opinion of the authors and not the opinion of the sponsor.

Appendix A. Elastic solution using large increment algorithm

For completeness, the solution of an elastic system using the large increment method will be presented here, since, the elastic solution is needed in the return algorithm. In their discussion, Aref and Guo (2001) present LIM as an optimization problem with the following statement,

$$\min \|\beta\delta\| \text{ subjected to } C_{m^*n}F_{n^*1} = P_{m^*1},$$

where

$$\delta = \varphi(F)$$

and the subscripts define the dimensions of C, F and P.

The goal of LIM is to search for a solution F to make $\|\beta\delta\|$ approach zero (i.e. a compatible solution). For solving the above optimization problem, we use the Lagrange multiplier method. First we form the Lagrangian function as,

$$L = \|\beta\delta\| + \lambda_1[C_{(1,1)}F_1 + C_{(1,2)}F_2 + \cdots + C_{(1,n)}F_n] + \cdots + \lambda_m[C_{(m,1)}F_1 + C_{(m,2)}F_2 + \cdots + C_{(m,n)}F_n],$$

where λ_i are the Lagrange multipliers. Then, we solve the following linear system of equations,

$$\frac{\partial L}{\partial F_i} = 0,$$
$$\frac{\partial L}{\partial \lambda_i} = 0.$$

The solution of this system of equations is the exact solution of the elastic system, which produces $\|\beta\delta\| = 0$.

References

ABAQUS, Hibbitt, Karlsson and Sorensen, Inc., Pawtucket, RI, 2003.

Aref, A.J., Guo, Z., 2001. Framework for finite-element-based large increment method for nonlinear structural problems. Journal of Engineering Mechanics 127 (7), 739–746.

Barham, W., Aref, A.J., Dargush, G.F., 2003. Derivation and implementation of a flexibility-based large increment method for solving non-linear structural problems. In: Proceedings of the Ninth International Conference on Civil and Structural Engineering Computing. Egmond-aan-Zee, The Netherlands.

Bathe, K., 1996. Finite Element Procedures. Prentice-Hall, Englewood Cliffs, NJ.

Ben-Israel, A., Greville, T., 1974. Generalized Inverse: Theory and Application. Wiley, New York.

Boisse, P.H., Ladeveze, P., Rougee, P., 1989. A large time increment method for elastoplastic problems. European Journal of Mechanics, A/Solids 8 (4), 257–275.

Boisse, P.H., Bussy, P., Ladeveze, P., 1990. A new approach in nonlinear mechanics: the large time increment method. International Journal for Numerical Methods in Engineering 29 (3), 647–663.

Clough, R.W., 1960. The finite element in plane stress analysis. In: Proceedings, 2nd ASCE Conference on Electrical Computation, Pittsburgh, PA.

Cook, R.D., Malkus, D.S., Plesha, M.E., 1989. Concepts and Applications of Finite Element Analysis. Wiley, New York.

Kaljevic, I., Patnaik, S.N., Hopkins, D.A., 1996. Development of finite elements for two-dimensional structural analysis using the integrated force method. Computers and Structures 59 (4), 691–706.

Ladeveze, P., 1999. Nonlinear Computational Structural Mechanics: New Approach and Non-Incremental Methods of Calculation. Springer Verlag, Prentice-Hall, NY.

Oden, J.T., 1972. Finite Elements of Nonlinear Continua. McGraw-Hill, New York.

Patnaik, S., 1973. An integrated force method for discrete analysis. International Journal for Numerical Methods in Engineering 6, 237–251.

Spacone, E., Ciampi, V., Filippou, F.C., 1996. Mixed formulation of nonlinear beam finite element. Computers and Structures 58 (1), 71–83.

Turner, M.J., Clough, R.W., Martin, H.C., Topp, L.J., 1956. Stiffness and deflection analysis of complex structures. Journal of Aeronautical Science 23, 805–823.

Zhang, C., Liu, X., 1997. A large increment method for material nonlinearity problems. Advances in Structural Engineering 1 (2), 99–109.